

****FULL TITLE****
*ASP Conference Series, Vol. **VOLUME**, **YEAR OF PUBLICATION***
****NAMES OF EDITORS****

Disk galaxies at $z=2$ in OWLS

Julio F. Navarro¹, Laura V. Sales², Joop Schaye³, Claudio Dalla Vecchia³ and Volker Springel⁴

¹ *Department of Physics and Astronomy, University of Victoria, Victoria, BC V8P 5C2, Canada.*

² *Kapteyn Astronomical Institute, P.O. Box 800, Groningen, The Netherlands.*

³ *Leiden Observatory, Leiden University, PO Box 9513, 2300 RA Leiden, The Netherlands*

⁴ *Max Planck Institute for Astrophysics, Karl-Schwarzschild-Strasse 1, 85740 Garching, Germany*

Abstract. We use the OWLS (Overwhelmingly Large Simulations) set of cosmological Nbody/gasdynamical simulations to study the properties of simulated galaxies at $z = 2$. We focus on the effect of supernova feedback from evolving stars on the baryonic mass and angular momentum content of galaxies that assemble at the center of 10^{11} - $10^{12} h^{-1} M_{\odot}$ halos. Our main finding is that the mass and angular momentum of such galaxies are strongly coupled, in a way that is approximately independent of feedback: varying the feedback implementation leads, in a given halo, to large variations in galaxy mass but leaves the galaxy mass-angular momentum correlation largely unaltered. In particular, the ratio between the angular momentum of a galaxy and that of its surrounding halo ($j_d = J_{\text{gal}}/J_{\text{vir}}$) correlates closely with the galaxy mass (expressed in units of the virial mass of the halo; $m_d = M_{\text{gal}}/M_{\text{vir}}$). This correlation differs substantially from the $m_d = j_d$ assumption commonly adopted in semianalytic models of galaxy formation. We use these results to infer the sizes of disk galaxies at $z = 2$ expected in the LCDM scenario and to interpret recent observations of extended disks at $z \sim 2$ by the SINS collaboration.

1. Introduction

It is widely thought that the properties of disk galaxies formed hierarchically (as expected in the prevailing LCDM paradigm) are largely determined by the properties of the dark matter halos in which they form. In this scenario, the scaling laws linking various disk galaxy properties, such as their mass, size, and rotation speed, simply reflect analogous correlations between the mass, spin, and potential depth of their surrounding halos (see, e.g., Navarro & Steinmetz 2000). Since the correlations linking various halo properties have been studied extensively through N-body simulations, the presumed association between disk and halo scaling laws enables a host of predictions for the properties of disk galaxies and their evolution with redshift. The general analytical framework has been developed in some detail by Mo, Mao & White (1998, hereafter MMW98), who showed that a number of properties of the present-day disk population

may be reproduced with well-motivated choices for the small number of free parameters in the model.

One important prediction of this modeling is that, at fixed rotation speed, disk galaxies should become smaller with increasing redshift. This prediction has come recently under scrutiny given the results of the SINS collaboration, who report the discovery of a population of extended disk galaxies at $z = 2$ (Genzel *et al.* 2006, Förster Schreiber *et al.* 2006). In some cases, these galaxies have rotation speeds comparable to L_* disks today and are as extended as their $z = 0$ counterparts. This in apparent contradiction with the predictions of the MMW98 modeling, unless these galaxies are embedded in halos with unusually high angular momentum (Bouché *et al.* 2007).

The interpretation of this disagreement is unclear, however, because N-body/gasdynamical simulations of galaxy formation have shown that a number of the assumptions made in the MMW98 model are not readily verified in the simulations. In particular, the mass and angular momentum of galaxies assembled hierarchically are not simple functions of the mass and spin of their surrounding halos (Navarro & Steinmetz 1997, 2000). The time of collapse; the importance of mergers; the feedback from evolving stars; all of these effects can alter dramatically the simple correspondence between galaxies and host halos envisioned in semianalytic models (Okamoto *et al.* 2005; Robertson *et al.* 2006; Governato *et al.* 2007). As a result, it is unclear whether the extended disks observed by the SINS collaboration present a challenge for the LCDM paradigm or whether they may be accommodated by reasonable tuning of the model free parameters.

We address these issues here using simulated galaxies selected from the Overwhelmingly Large Simulations (OWLS) project. We use these simulations to examine the relation between mass and angular momentum (and its dependence on feedback) in $z = 2$ galaxies assembled in the LCDM scenario. We use these results to validate the MMW98 model and to compare with the results from the SINS collaboration.

2. The numerical simulations

The Overwhelmingly Large Simulation (OWLS) project is a collection of roughly 50 Nbody/gasdynamical cosmological simulations of representative volumes in an LCDM universe. The various OWLS runs explore systematically the effect on the simulated galaxy population of varying numerical resolution, star formation laws, cooling function, sub-grid physics, and feedback recipes.

We select for this study four different OWLS runs that differ from each other only in the way supernova (SN) feedback is implemented. Each run follows the evolution of 512^3 dark matter and 512^3 gas particles in a $25 h^{-1}$ Mpc box. The mass per particle in these runs is $\sim 6 \times 10^6 h^{-1} M_\odot$ for the dark matter and six times lower for the baryons. Gas is allowed to cool radiatively, and to turn into stars in a manner consistent with an empirically calibrated Schmidt-Kennicutt law. Feedback energy from evolving stars is incorporated assuming that a fixed fraction of the available energy (40% of the total energy released by SN for a Chabrier IMF) is channeled into bulk motions of the gas particles in order to mimic feedback-driven “winds” outflowing from regions of active star formation.

In all four runs the same amount of energy is invested in feedback; the main differences between runs are the choices made for the wind velocity (v_w) and mass loading (η) factor. The parameter η specifies the number of gas particles among which the feedback kinetic energy is split, whereas v_w characterizes the outflow velocity of the wind particles.

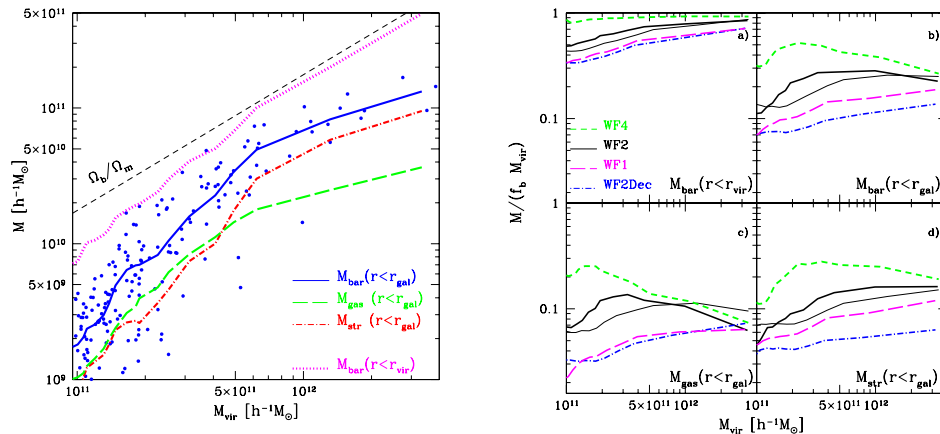


Figure 1. *Left:* Galaxy mass as a function of halo virial mass for galaxies in the WF2 run. The various curves are described in the text, and trace medians in equal-number bins of virial mass. Dot-dashed, dashed, and solid lines correspond to stars, gas and all baryons (=gas+stars), respectively. Individual values are shown for the gas+stars case, in order to illustrate the halo-to-halo scatter. *Right:* Galaxy mass in units of the total baryon mass of the halo. Different curves in each panel correspond to runs with different feedback implementation. Clockwise from the top left, each panel shows (a) the baryonic mass within the virial radius; (b) the baryonic mass in the central galaxy (i.e., within r_{gal}); (c) the stellar mass within r_{gal} , and (d) the gaseous mass within r_{gal} . The thin solid line correspond to a run with the same parameters as WF2 but with 8 times fewer particles, a good indicator of numerical convergence.

For the range of halo masses investigated here the effects of feedback (in terms of how effectively it regulates star formation and/or removes gas from galaxies) increase with v_w for fixed $\eta \times v_w^2$. We refer to each of the 4 runs, in order of increasing overall feedback efficiency, as: WF4 ($\eta = 4$ particles and $v_w = 424$ km/s), WF2 ($\eta = 2$ and $v_w = 600$ km/s), WF1 ($\eta = 1$ and $v_w = 848$ km/s) and WF2Dec. The latter is equivalent to WF2 but “wind” particles are temporarily decoupled from the hydrodynamical equations (see Dalla Vecchia & Schaye 2008 for details).

Our simulated galaxy sample consists of all galaxies assembled (at $z = 2$) at the centers of dark halos in the mass range $M_{\text{vir}} = 10^{11}$ to $3 \times 10^{12} h^{-1} M_{\odot}$. These halos contain between 50,000 and 500,000 particles within the virial radius (defined as the radius where the mean inner density is $\Delta = 178$ times the critical density of the universe at $z = 2$). The gravitational softening is never greater than $0.5 h^{-1} \text{kpc}$ (physical). With these definitions, the simulated galaxy sample in each run contains roughly ~ 170 objects.

3. Results

3.1. Mass and angular momentum content

The left panel of Fig. 1 shows, as a function of halo virial mass, the baryonic mass in various components for galaxies identified in the WF2 run. The (top) dashed straight line indicates the baryon mass associated with each halo through the universal baryon fraction $f_b = \Omega_b/\Omega_M$. The bottom four curves show the baryon mass in different regions of the halo. The dotted line corresponds to all baryons within r_{vir} . This shows that halos at the high-mass end of the considered range are able to retain all baryons but that those at the low mass end have experienced a net loss of about $\sim 50\%$ of their baryons. This illustrates the decreasing efficiency of feedback-driven winds in the deeper potential wells of more massive halos.

The effect is even more pronounced when considering the total amount of baryons locked in the central galaxy (i.e., those within $r_{\text{gal}} = 0.1 r_{\text{vir}}$ from the halo centre). The dots in the left panel of Fig. 1 show that the total baryon mass of the central galaxy is not simply proportional to the halo mass. The relation has substantial scatter and it varies systematically as a function of M_{vir} . (All curves in this plot trace the median in equal-number bins of virial mass.) At low M_{vir} central galaxies collect on average only about 10% of the baryon mass associated with the halo through the universal baryon fraction. This fraction rises to almost 50% for $6 \times 10^{11} h^{-1} M_{\odot}$ halos, but appears to decline in more massive halos.

The decline at the high-mass end is likely a result of the longer cooling times characteristic of massive halos, which hinder the assembly of massive central galaxies. The bottom two curves indicate how the baryon mass of central galaxies splits into gas (dashed) and stars (dot-dashed). Gas and stars contribute about equally at low masses, but central galaxies in high-mass halos are predominantly stellar. This is presumably a result of the inability of feedback to delay or prevent the efficient conversion of gas into stars in halos with a deep potential well. The effect on these trends of different feedback prescriptions may be seen on the right panel of Figure 1. Clearly, variations in feedback implementation have a large effect on the mass (and gas fraction) of central galaxies. In low mass halos (e.g., $M_{\text{vir}} \sim 2 \times 10^{11} h^{-1} M_{\odot}$) WF4 and WF2Dec galaxies differ by more than a factor of 5, illustrating the wide range of feedback efficiency surveyed in the OWLS simulations.

The left panel of Fig. 2 shows the *specific* angular momentum as a function of halo mass for various components in the WF2 galaxy sample. The dark matter angular momentum scales roughly as $j_{\text{drk}} \propto M^{2/3}$; the expected scaling for systems with similar dimensionless spin parameter λ . This scaling is followed closely by all baryons within the virial radius (dotted line), a result that illustrates the fact that both baryons and dark matter were torqued and spun by the same amount during the early expansion phase of each system (see, e.g., Navarro et al 2004).

By comparison, the baryons in the central galaxies have much lower specific angular momentum; a factor of ~ 3 lower on average (solid curve and dots in the left panel of Fig. 2). It is also clear from this figure that the gas (dashed curve) has typically higher angular momentum than the stars (dot-dashed). This

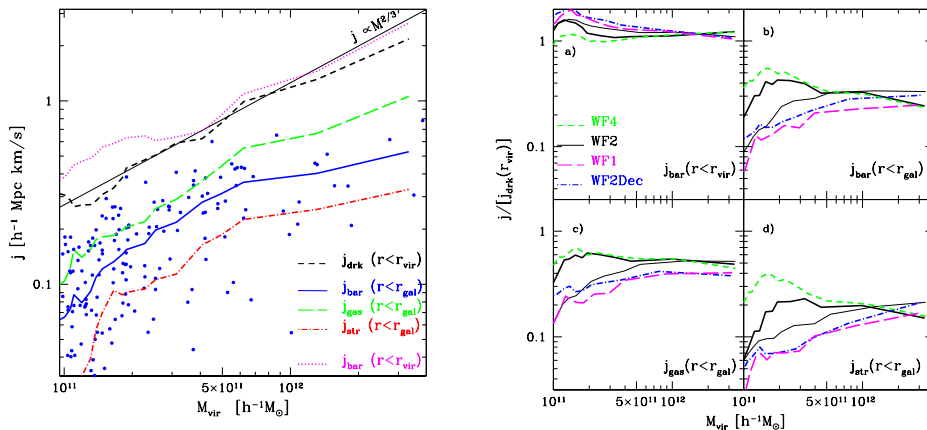


Figure 2. *Left:* Specific angular momentum (j) as a function of halo virial mass in the WF2 galaxy sample. Line types are as in Fig. 1. The dashed black curve shows that the specific angular momentum of the dark halo scales roughly as $M^{2/3}$, as expected for systems with constant dimensionless spin parameter λ . The bottom curves show the specific angular momentum of stars (red dot-dashed), gas (green long-dashed) and all baryons (blue solid) within r_{gal} . The mean angular momentum of all baryons within the virial radius ($j_{\text{bar}}(r < r_{\text{vir}})$) is shown in magenta dotted line. *Right:* Specific angular momentum of various components expressed in units of the halo's, as a function of halo virial mass. Different lines in each panel correspond to various feedback prescriptions, as described in the caption to Fig. 1.

reflects the higher efficiency of transformation of gas into stars in the central (denser) regions of a galaxy and implies that gaseous disks will be, on average, larger than stellar ones. As we discuss below, it is important to take this effect into account when comparing theoretical predictions with observations.

These trends are common to all our feedback implementations, as may be verified by inspecting the right panel of Fig. 2. Note, however, that feedback affects the mass and angular momentum of central galaxies in different ways. Indeed, compare the central galaxy masses (top-right panel of Fig. 1) and spins (top right panel of Fig. 2) of models WF4 and WF2Dec, our most and least efficient feedback runs, respectively. In high-mass halos the baryonic mass of WF4 central galaxies is roughly ~ 2 -3 larger than in WF2Dec, but its specific angular momentum remains largely unchanged.

This non-linear interplay between the mass and spin of the baryons that are assembled into central galaxies is explored in Fig. 3, where we show the galaxy's mass ($m_d = M_{\text{gal}}/M_{\text{vir}}$) and angular momentum ($j_d = J_{\text{gal}}/J_{\text{vir}}$), each expressed in units of the corresponding halo values. Semianalytic models of galaxy formation typically assume that the specific angular momentum of the central galaxy is similar to that of its host halo; i.e., that $m_d = j_d$. In the MMW98 formalism, these parameters enable prediction of the exponential scalelength of a disk galaxy once the virial radius (r_{vir}) and spin parameter (λ) of a halo are specified,

$$R_d = (2f_c)^{-1/2} (j_d/m_d) \lambda r_{\text{vir}} f_R(j_d, m_d, c, \lambda), \quad (1)$$

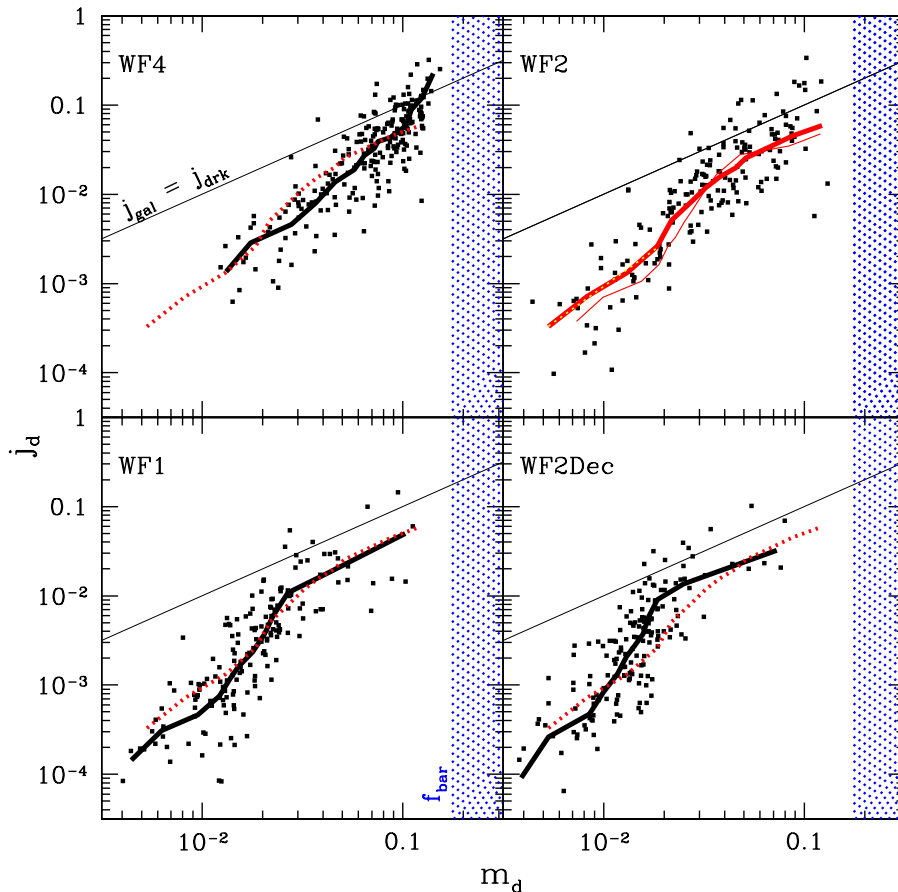


Figure 3. Baryonic mass $m_d = M_{\text{gal}}/M_{\text{vir}}$ and angular momentum $j_d = J_{\text{gal}}/J_{\text{vir}}$ of central galaxies, in units of the halo virial mass and angular momentum. Each panel corresponds to a different feedback prescription. Thick lines in each panel show the median j_d in equal-number m_d bins for each run. (The thin line in the WF2 panel corresponds to a similar simulation with 8 times fewer particles.) The red dotted line, corresponding to WF2, is repeated in all panels, and highlights our result that the m_d - j_d relation is approximately independent of feedback efficiency. The blue shaded area shows the region where the central galaxy mass would exceed the baryon mass within r_{vir} ; i.e., $m_d > f_{\text{bar}}$. No galaxies are expected (or seen) in this region of the plot.

where f_R and f_c are factors that account for the concentration and “contraction” of the dark halo.

The m_d - j_d relation in our simulations is shown in Fig. 3, where each panel corresponds to a different feedback implementation. A few things are worth noting in this figure. (i) Simulated galaxies deviate strongly from the $m_d = j_d$ line, which assumes that galaxies and halos have the same specific angular momentum (i.e., $j_{\text{gal}} = j_{\text{drk}}$). (ii) The scatter in the relation is large, and in every

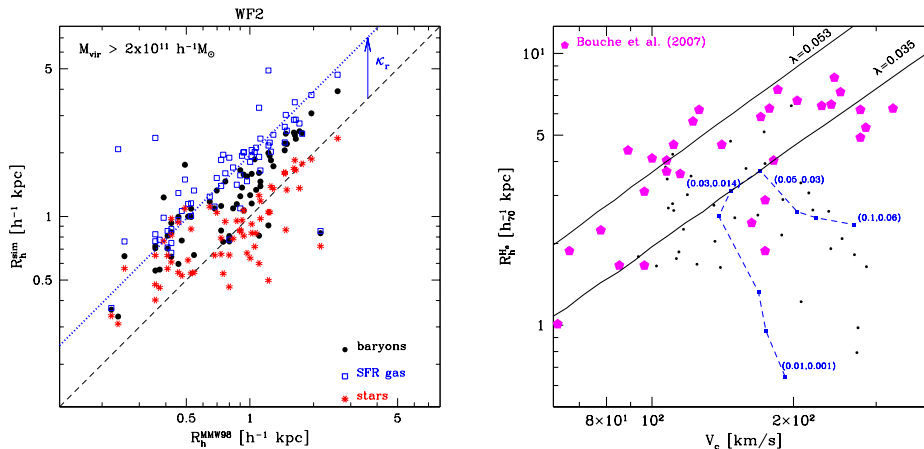


Figure 4. *Left:* Cylindrical half-mass radii predicted by the MMW98 formalism (x-axis) versus projected half-mass radius of simulated galaxies. Stars are shown by red asterisks, star-forming gas by empty blue squares, and all baryons by solid black dots. *Right:* The size-velocity plane of $z = 2$ SINS galaxies (magenta pentagons), together with the prediction of MMW98 for disks in a halo with $V_{\text{vir}} = 150$ km/s, average concentration, and spin parameter $\lambda = 0.035$. The disk parameters m_d and j_d are assumed to follow the median m_d - j_d relation found in the simulations. The solid black curves outline the size-velocity relation expected for disks with $(m_d, j_d) = (0.05, 0.03)$ in halos with $\lambda = 0.035$ and 0.053 , respectively. Black dots correspond to a subset of our simulated galaxies with m_d - j_d values close to the values that maximize disk size: $m_d = 0.05$ and $j_d = 0.03$. These show that extended disks are indeed present at $z = 2$ in our simulations.

panel there are cases where $j_{\text{gal}} > j_{\text{drk}}$. These are galaxies where feedback has been able to push out a substantial fraction of low-angular momentum baryons. As a result, those that remain attached to the central galaxy have specific angular momentum higher than the system as a whole. (iii) Feedback efficiency largely determines m_d : for example, WF4 galaxy masses are on average 3 to 5 times larger than WF2Dec galaxies. This may be seen as a horizontal shift of points between the corresponding panels. (iv) The m_d - j_d relation is approximately independent of feedback. This is illustrated by the dotted curve, which is repeated in each panel, and which reproduces the median j_d as a function of m_d in the WF2 run. This curve approximates reasonably well the j_d - m_d relation in *all* panels. In other words, for the feedback implementation adopted in our simulations the fraction of baryons that collects into the central galaxy is the primary factor determining the angular momentum content this galaxy retains.

3.2. Implications for disk galaxy sizes

We may also use our simulations to check the validity of the MMW98 formula for predicting galaxy sizes. This is shown in the left panel of Fig. 4, where we plot the predicted (cylindrical) half-mass radius (R_h^{MMW98}) versus the projected half-mass radius of stars (red asterisks), star-forming gas (empty blue squares) and baryons (black circles), for galaxies identified in the WF2 simulation.

The agreement is quite good for the stellar component, which is striking given the number of simplifying assumptions that go into the prediction and that are not matched in detail by the simulations. For example, the MMW98 prediction assumes that all baryons are in a centrifugally-supported exponential disk; simulated galaxies, on the other hand, exhibit a very wide range of disk-to-spheroid ratio. Interestingly, when scaled by a constant factor $\kappa_r \sim 2$ the MMW98 formula also predicts rather accurately the size of the star-forming *gaseous* disks (see upper dotted curve in the left panel of Fig. 4).

We can combine this result with the m_d - j_d relation discussed above to compute the expected size of (gaseous) disks at $z = 2$. As shown in the right panel of Fig. 4, the disk size and rotation speed depend sensitively on j_d and m_d . The jagged curve in this panel shows how the size of gaseous disks formed in a halo of *fixed* virial velocity $v_{\text{vir}} = 150$ km/s changes as j_d and m_d are varied. The halo is assumed to have average concentration for its mass, and average spin, $\lambda = 0.035$. The jagged curve maps, in the disk size-rotation speed plane, variations in (m_d, j_d) chosen to lie along the relation shown by the dotted line in Fig. 3, from $(0.01, 0.001)$ to $(0.1, 0.06)$. The disk radius depends critically on the value of j_d and m_d : *disk sizes vary by a factor of ~ 8 , even though the halo mass, concentration, and spin are fixed.*

For small values of j_d the central disk has very little angular momentum, and therefore a rather small size. As j_d (and m_d) increases, the disk grows steadily in size. Disk radii are maximized for $m_d = 0.05$ and $j_d = 0.03$ in this example. Increasing j_d further results in massive disks (because of the concurrent rise in m_d) with very high rotation speeds. Since angular momentum scales as disk size times rotation speed, these massive disks end up being actually smaller, despite their larger j_d . Clearly, predicting the size of disks is a rather uncertain endeavour unless one is able to constrain the values of the parameters j_d and m_d to within a very narrow range.

As may be seen in Fig. 4, disks in $V_{\text{vir}} = 150$ km/s halos may reach a size of order $\sim 4 h_{70}^{-1}$ kpc, comparable to the size of disks in the SINS sample. (SINS data are shown by large pentagons in the right-hand panel of Fig. 4.) Larger disks may also exist, for example, in more massive (intrinsically larger) halos, or in halos with higher-than-average λ , or in systems where galaxies have retained an unusually high fraction of its angular momentum (i.e., those that scatter *above* the mean m_d - j_d relation in Fig. 3). Taking, as an example, the WF2 run, we find, at $z = 2$, about 5×10^{-3} gaseous disks exceeding $\sim 2 h_{70}^{-1}$ kpc (physical) in size per cubic h^{-1} Mpc (comoving). These numbers are in rough agreement with the findings of the SINS collaboration (Bouché et al 2007). We hasten to add that these are not “typical” galaxies at that redshift, but rather some of the largest ones present then. The selection of SINS galaxies favors large disks in order to enhance the probability of obtaining a resolved velocity map, and therefore they cannot be considered “average” at that redshift either. The presence of a (reasonable!) number of extended disks at $z = 2$ might thus not require unusually high halo spins nor present an insurmountable challenge to the LCDM structure formation paradigm.

References

- Bouché N., et al. 2007, ApJ, 671, 303
Dalla Vecchia C., Schaye J., 2008, MNRAS, 387, 1431
Dutton A. A., van den Bosch F. C., 2008, ArXiv e-prints
Förster Schreiber N., et al. 2006, ApJ, 645, 1062
Genzel, R., et al. 2006, Nat, 442, 786
Governato, F., et al 2007, MNRAS, 374, 1479
Mo H. J., Mao S., White S. D. M., 1998, MNRAS, 295, 319
Navarro, J. F., & Steinmetz, M. 1997, ApJ, 478, 13
Navarro J. F., Steinmetz M., 2000, ApJ, 538, 477
Navarro, J. F., Abadi, M. G., & Steinmetz, M. 2004, ApJ, 613, L41
Okamoto T., Eke V. R., Frenk C. S., Jenkins A., 2005, MNRAS, 363, 1299
Robertson B., et al 2006, ApJ, 645, 986